Multiscale analysis of wave propagation in random media

Josselin Garnier*

Abstract

Wave propagation in random media can be studied by multiscale and stochastic analysis. We review some recent advances and their applications. In particular, in a physically relevant regime of separation of scales, wave propagation is governed by a Schrödinger-type equation driven by a Brownian field. We study the associated moment equations and describe the propagation of coherent and incoherent waves. We quantify the scintillation of the wave and the fluctuations of the Wigner distribution. These results make it possible to introduce and characterize correlation-based imaging methods.

1 Wave propagation in random media

In many wave propagation scenarios the medium is not constant, but varies in a complicated fashion on a spatial scale that is small compared to the total propagation distance. This is the case for wave propagation through the turbulent atmosphere and complex biological tissue for instance. If one aims to use transmitted or reflected waves for communication or imaging purposes it is important to characterize how such microstructure affects and corrupts the wave.

Motivated by the situation described above we consider wave propagation through time-independent complex media with a spatially varying index of refraction. Typically we cannot expect to know the index of refraction pointwise so we model it as a realization of a random process. When the index of refraction is a random process, the wave field is itself a random process and we are interested in how the statistics of the random medium affects the statistics of the wave field. The analysis of wave propagation in random media has a long history. It was first dealt with phenomenogical models such as the radiative transfer theory. The first mathematical papers were written in the 60's by J. Keller [35] who connected radiative transport theory and random wave equations. In the review [42] presented by G. Papanicolaou at ICM in 1998, the main focus was on wave transport and localization (when random inhomogeneities are strong enough to trap wave energy in a bounded region). The book [17] gives the state of the art about wave propagation in randomly layered media, that is a situation mathematically tractable and physically relevant (especially in geophysics). In the recent years several new features have emerged. 1) First statistical stability has become a central issue. Indeed the modeling of a complex medium by a random medium involves ensemble averages. In some circumstances, such as

*Centre de Mathématiques Appliquées, Ecole Polytechnique, 91128 Palaiseau Cedex, France josselin.garnier@polytechnique.edu

the turbulent atmosphere or the ocean, the medium may change (slowly) in time so that ensemble averages can be experimentally achieved. This is not the case in other configurations, such as seismology, in which the Earth is not moving although it can be considered as a realization of a random medium to model uncertainty and lack of information. It is then important to look for statistically stable quantities, that is to say, quantities that depend on the statistics of the random medium that can be known or estimated, but not on the particular realization that is inaccessible. To quantify statistical stability, variance calculations are required, which are based on high-order moment analysis.
2) Motivated by statistical stability analysis and time-reversal experiments for waves in random media, new methods for communication and imaging have been introduced that are based on wave field correlations. The understanding and analysis of these methods again require high-order moments calculations.
3) Following the analysis of wave field correlations, it was understood that information about the medium could be extracted from wave correlations even when the illumination is provided not by controlled sources, but by uncontrolled, opportunistic or ambient noise sources.
A common feature of these recent developments is the analysis and use of wave field correlations that reveal very rich information. Modern imaging techniques such as seismic interferometry [49, 48, 60] or coherent interferometric imaging [7, 8] correlate wave field traces that have been corrupted by the microstructure of the medium and use their space-time correlation function for imaging.

1.1 Multiscale analysis

In its most common form, the analysis of wave propagation in random media consists in studying the wave field solution of the scalar time-harmonic wave or Helmholtz equation with a randomly heterogeneous index of refraction. Even though the scalar wave equation is simple and linear, the relation between the statistics of the index of refraction and the statistics of the wave field is highly nontrivial. In order to simplify and understand this relation, one can carry out a multiscale analysis that will transform the random Helmholtz equation into a mathematically tractable yet physically relevant problem. This analysis is based on a separation of scales technique and limit theorems (homogenization, diffusion-approximation, ...), in the framework set forth by G. Papanicolaou and coauthors [1]. The wave propagation problem can, indeed, be characterized by several length scales: the typical wavelength (which depends on the source), the correlation radius of the medium, the typical propagation distance. The bandwidth of the source and the relative amplitude of the medium fluctuations may also play a role. Different scaling regimes (corresponding to different physical configurations) can be analyzed when certain ratios between these length scales go to zero or infinity. They lead to tractable and relatively easy to interpret asymptotic results. Typically, the solution of the random Helmholtz equation can be shown to converge to the solution of a deterministic or stochastic partial differential equation driven by a Brownian field as in the situation addressed in Section 2. Stochastic calculus can then be used to compute quantities of interest.

In the random travel time model, which is a special high-frequency regime in which the

wavelength is much smaller than the correlation radius of the medium, the fluctuations of the medium affect only the phase of the wave, which satisfies a random eikonal equation [9, 53]. In the random paraxial model in which the wavelength is smaller than the correlation radius of the medium, backscattering can be neglected but there is significant lateral scattering as the wave advances over long propagation distances and the wave field satisfies a random Schrödinger-type equation [52, 55]. In the randomly layered regime, the medium is only varying along the longitudinal direction (along the propagation axis), there is significant backscattering and the plane wave mode amplitudes satisfy a system of ordinary random differential equations [17]. In the radiative transport regime, in which the wavelength is of the same order as the correlation radius of the medium, the angular distribution of the mean wave energy satisfies a transport equation [46, 47].

In this review paper we consider a scaling regime corresponding to long-range high-frequency beam propagation and small-scale medium fluctuations giving negligible backscattering. This is the so-called white-noise paraxial regime, as described by the Itô-Schrödinger model, which is presented in Section 2. This model is a simplification of the random Helmholtz equation since it corresponds to an evolution problem, but yet in the regime that we consider it describes the propagated field in a weak sense in that it gives the correct statistical structure of the wave field. The Itô-Schrödinger model can be derived rigorously from the random Helmholtz equation by a separation of scales technique in the high-frequency regime (see [2] in the case of a randomly layered medium and [24, 25, 26] in the case of a three-dimensional random medium). It models many situations, for instance laser beam propagation [51], underwater acoustics [52], or migration problems in geophysics [11]. The Itô-Schrödinger model makes it possible to use Itô's stochastic calculus, which in turn enables the closure of the hierarchy of moment equations [18, 33]. The equations for the first-order and second-order moments are easy to solve. The equation for the fourth-order moments is difficult and only approximations or numerical solutions have been available for a long time (see [14, 54, 56] and [33, Sec. 20.18]). In a special scaling regime, it is, however, possible to derive expressions for the fourth-order moments as presented in Section 3.

The results on the higher-order statistics of the wave field open the mathematical analysis of important problems. Below we discuss a few applications, from the understanding of physical conjectures such as star scintillation to the design of efficient correlation-based imaging schemes in complex media. We believe that many more problems than those mentioned here will benefit from the results regarding the statistics of the wave field. In fact, enhanced transducer technology and sampling schemes allow for using finer aspects of the wave field involving second- and fourth-order moments and in such complex cases a rigorous mathematical analysis is important to support, complement, or sometimes disprove, statements based on physical intuition alone.

1.2 A few conjectures

Star scintillation is a well-known paradigm, related to the observation that the irradiance of a star fluctuates due to interaction of the light with the turbulent atmosphere. Experimental observations indicate that the statistical distribution of the irradiance is

exponential, with the irradiance being the square magnitude of the complex wave field. In the physical literature it is a well-accepted conjecture that the statistics of the complex wave field becomes circularly symmetric complex Gaussian when the wave propagates through the turbulent atmosphere [58, 61], so that the irradiance is the sum of the squares of two independent real Gaussian random variables, which has chi-square distribution with two degrees of freedom, that is an exponential distribution. The mathematical proof of this conjecture has been obtained in randomly layered media [17, Chapter 9] but is still incomplete in three-dimensional random media [18, 27, 28]. In Section 4 we report results for the fourth-order moments that are consistent with the Gaussian conjecture.

Certain functionals of the wave field carry information about the medium and can be characterized in some specific regimes [3, 4, 13, 44]. For instance, the Wigner distribution (a transform in time-frequency analysis) is known to be convenient to study the solution of Schrödinger equation [30, 46]. An important issue is the so-called statistical stability property: we look for functionals that become deterministic in the considered scaling regime and that depend only on the statistics of the random medium and not on the particular realization. The conjecture is that this can happen for well chosen functionals in the limit of rapid decorrelation of the medium fluctuations. In [36, 37] the authors consider a situation with rapidly fluctuating random medium fluctuations in which the Wigner distribution is statistically stable. As shown in [3], however, the statistical stability also depends on the initial data and can be lost for very rough initial data even with a high lateral diversity as considered there. In Section 5 we present a detailed and quantitative analysis of the stability of the Wigner distribution and derive an explicit expression of the coefficient of variation of the smoothed Wigner distribution as a function of the smoothing parameters, in the general situation in which the standard deviation can be of the same order as the mean. This is a realistic scenario, which is not too deep into a statistical stabilization situation, but which gives partly coherent but fluctuating wave functionals. These results make it possible to quantify such fluctuations and how their magnitudes can be controlled by optimal smoothing of the Wigner distribution.

1.3 Applications to communication and imaging

The understanding of the statistics of the wave field is very important for applications to communication and imaging. Many studies are driven by practical considerations or experimental observations.

1) The time-reversal experiments carried out by M. Fink and his group have motivated many theoretical developments [16]. These experiments are based on the use of a special device called a time-reversal mirror (TRM). A TRM is an array of transducers, that is to say, an array of sensors that can be used as sources and as receivers. A time-reversal experiment has two steps. In the first step, the TRM is used as an array of receivers. A wave is transmitted by a point source far away from the TRM and is recorded by the TRM. In the second step, the TRM is used as an array of sources. It transmits the time-reversed recorded signals. The main observations are that i) the wave refocuses on the original source location, ii) refocusing is enhanced when the medium is randomly scattering, and iii) the time-reversed refocused wave is statistically stable, in the sense that the profile of

the focal spot depends on the statistical properties of the random medium, but not on its particular realization. The phenomenon of focusing enhancement has been analyzed quantitatively [6, 43, 17]. Statistical stability of time-reversal refocusing for broadband pulses is usually qualitatively proved by the fact that the time-reversed refocused wave is the superposition of many frequency-dependent components that are uncorrelated, which gives the self-averaging property by the law of large numbers [6, 43]. For narrowband pulses the analysis of the statistical stability phenomenon involves the evaluation of a fourth-order moment of the Green's function of the random wave equation. This problem has been addressed in [34] by using the circular complex Gaussian assumption without rigorous justification. It is, however, possible to prove that the fourth-order moments satisfy Isserlis formula (i.e. they can be expressed in terms of sums of products of second-order moments) and to give a detailed analysis of the statistical stability of the time-reversed refocused wave [28].

2) Wavefront-shaping-based schemes [59] have attracted a lot of attention in recent years. The primary goal is to focus monochromatic light through a layer of strongly scattering material. This is a challenging problem as multiple scattering of waves scrambles the transmitted light into random interference patterns called speckle patterns [32]. By using a spatial light modulator (SLM) before the scattering medium (a device that can modulate the intensity and/or the phase profile of the light beam), it is possible to focus light as first demonstrated in [59]. Indeed, the elements of the SLM can impose prescribed phase shifts, and an optimization scheme makes it possible to choose the phase shifts so as to maximize the intensity transmitted at one target point behind the scattering medium. The optimal phase shifts are the opposite phases of the field emitted by a point source at the target point and recorded in the plane of the SLM [40]. In other words, the wavefront-shaping optimization procedure is equivalent to phase conjugation or time reversal. Moreover, it has been shown that the speckle memory effect [15, 19] allows to focus on a neighboring point close to the original target point [59], which opens the way to the transmission of spatial patterns [45]. This phenomenon can be quantified by fourth-order moments calculations as shown in [29].

3) In imaging in complex media, when the propagation distance is large enough, the cross correlations of the recorded signals play an important role. This is because the mean (or coherent) field vanishes while the correlations carry information about the medium through which the waves propagate (see Section 3 in the random paraxial regime). The mathematical analysis aims at two goals. First one needs to understand how information about the medium is encoded in the wave field correlations. Second one needs to determine how this information can be extracted in a statistically stable way. This requires detailed fourth-order moment calculations. These calculations help determining imaging functions that can operate in scattering media (see [9, 20] for instance).

4) Intensity correlations is a recently proposed scheme for communication and imaging in the optical regime. Indeed, in optics only intensities (i.e. the square moduli of the complex envelopes of the wave fields) can be recorded. Intensity correlation-based imaging is a promising scheme for communication and imaging through relatively strong clutter. By using the correlation of the intensity or speckle for different incoming angles, or different positions of the source, or different output angles, one can get spatial information about

the source [41]. The idea of using the information about the statistical structure of speckle to enhance signaling is very interesting and corroborates the idea that modern schemes for communication and imaging require a mathematical theory for analysis of high-order moments.

5) In conventional imaging the waves are generated by an active array of sources and after propagation through the medium they are recorded by an array of receivers (that can be collocated or not with the array of sources). In passive imaging, only receiver arrays are used and the illumination is provided by unknown, uncontrolled, asynchronous, or opportunistic sources. From a theoretical point of view the cross correlations between the recorded signals carry information about the medium through which the waves propagate, as we explain in Section 6. Therefore they play an important role in passive imaging and they can be used for travel-time tomography and reflector imaging [23]. From an applied point of view the emergence of correlation-based imaging using ambient seismic noise has had a profound impact in seismology, as can be seen in the work of M. Campillo and co-workers [49]. The use of seismograms generated by earthquakes was previously the only way to image the Earth. With correlation-based imaging, the seismic noise recorded by a distributed network of sensors on the surface of the Earth can provide a lot of information about its structure. Beyond seismology, there are many new, emerging areas for correlation-based imaging methods, in passive synthetic aperture radar or in optical speckle intensity correlations for communications and imaging. We introduce and explain one of these methods called ghost imaging in Section 7.

2 The white-noise paraxial model

In this section we describe how to derive the mathematically tractable Itô-Schrödinger model from the wave equation in a random medium. We consider the three-dimensional scalar wave equation:

$$\frac{1}{c^2(\vec{\boldsymbol{x}})}\frac{\partial^2 u}{\partial t^2}(t,\vec{\boldsymbol{x}}) - \Delta_{\vec{\boldsymbol{x}}} u(t,\vec{\boldsymbol{x}}) = F(t,\vec{\boldsymbol{x}}), \qquad t\in\mathbb{R}, \quad \vec{\boldsymbol{x}}\in\mathbb{R}^3. \tag{1}$$

Here the source emits a time-harmonic signal with frequency ω and it is localized in the plane $z=0$:

$$F(t,\vec{\boldsymbol{x}}) = \delta(z) f(\boldsymbol{x}) e^{-i\omega t}, \text{ with } \vec{\boldsymbol{x}} = (\boldsymbol{x},z)\in\mathbb{R}^2\times\mathbb{R}, \tag{2}$$

and the speed of propagation is spatially heterogeneous

$$\frac{1}{c^2(\vec{\boldsymbol{x}})} = \frac{1}{c_o^2}\big(1+\mu(\vec{\boldsymbol{x}})\big), \tag{3}$$

where μ is a zero-mean stationary random process with ergodic properties.

The time-harmonic field $\hat{u}$ such that $u(t,\vec{\boldsymbol{x}}) = \hat{u}(\vec{\boldsymbol{x}})e^{-i\omega t}$ is solution of the random Helmholtz equation

$$(\partial_z^2 + \Delta_\perp)\hat{u} + \frac{\omega^2}{c_o^2}\big(1+\mu(\boldsymbol{x},z)\big)\hat{u} = -\delta(z) f(\boldsymbol{x}),$$

where $\Delta_{\vec{\boldsymbol{x}}} = \Delta_\perp + \partial_z^2$. The function $\hat{\phi}$ (slowly-varying envelope of a plane wave going along the z-axis) defined by

$$\hat{u}(\boldsymbol{x}, z) = \frac{ic_o}{2\omega} e^{i\frac{\omega z}{c_o}} \hat{\phi}\big(\boldsymbol{x}, z\big) \tag{4}$$

satisfies

$$\partial_z^2 \hat{\phi} + \left(2i\frac{\omega}{c_o}\partial_z \hat{\phi} + \Delta_\perp \hat{\phi} + \frac{\omega^2}{c_o^2}\mu\big(\boldsymbol{x}, z\big)\hat{\phi}\right) = 2i\frac{\omega}{c_o}\delta(z) f(\boldsymbol{x}). \tag{5}$$

In the paraxial regime "$\lambda \ll \ell_c, r_o \ll z$" (which means, the wavelength $\lambda = 2\pi c_o/\omega$ is much smaller than the correlation radius ℓ_c of the medium and the radius r_o of the source, which are themselves much smaller than the propagation distance z) the forward-scattering approximation in direction z is valid and $\hat{\phi}$ satisfies the Itô-Schrödinger equation [25]

$$\mathrm{d}_z \hat{\phi} = \frac{ic_o}{2\omega}\Delta_\perp \hat{\phi}\,\mathrm{d}z + \frac{i\omega}{2c_o}\hat{\phi} \circ \mathrm{d}B(\boldsymbol{x}, z), \qquad \hat{\phi}(z=0, \boldsymbol{x}) = f(\boldsymbol{x}), \tag{6}$$

where $\circ$ stands for the Stratonovich integral, $B(\boldsymbol{x}, z)$ is a Brownian field, that is a Gaussian process with mean zero and covariance

$$\mathbb{E}[B(\boldsymbol{x}, z)B(\boldsymbol{x}', z')] = \gamma(\boldsymbol{x} - \boldsymbol{x}')\min(z, z') \text{ with } \gamma(\boldsymbol{x}) = \int_{\mathbb{R}} \mathbb{E}[\mu(\boldsymbol{0}, 0)\mu(\boldsymbol{x}, z)]\mathrm{d}z. \tag{7}$$

Remark: Existence, uniqueness and continuity of solutions of the Itô-Schrödinger model (6) are established in [12]. The proof of the convergence of the solution to (5) to the solution to (6) is in [25]. A first proof in the case of layered media (i.e. when $\mu \equiv \mu(z)$) can be found in [2]. More precisely, the paraxial regime "$\lambda \ll \ell_c, r_o \ll z$" corresponds to the scaled regime

$$\omega \to \frac{\omega}{\varepsilon^4}, \qquad \mu(\boldsymbol{x}, z) \to \varepsilon^3 \mu\big(\frac{\boldsymbol{x}}{\varepsilon^2}, \frac{z}{\varepsilon^2}\big), \qquad f(\boldsymbol{x}) \to f\big(\frac{\boldsymbol{x}}{\varepsilon^2}\big),$$

where ε is a small dimensionless parameter, and the convergence in $\mathcal{C}([0,\infty), L^2(\mathbb{R}^2))$ (or in $\mathcal{C}([0,\infty), H^k(\mathbb{R}^2))$) of the solution of the scaled version of (5) to the solution of the Itô-Schrödinger equation (6) holds in distribution when $\varepsilon \to 0$. This result requires strong mixing properties for the random process μ. If, however, the process μ has long-range properties, in the sense that $\mathbb{E}[\mu(\boldsymbol{x}, z)\mu(\boldsymbol{x}', z')] = r(z - z')\gamma(\boldsymbol{x} - \boldsymbol{x}')$ with $r(z) \sim c_\alpha |z|^{-\alpha}$ as $|z| \to +\infty$ and $\alpha \in (0, 1)$, then, under appropriate technical and scaling assumptions [31], the limiting equation is the fractional Itô-Schrödinger model (6) in which B is a fractional Brownian field with Hurst index $H = 1 - \alpha/2 \in (1/2, 1)$, i.e. a Gaussian field with mean zero and covariance

$$\mathbb{E}[B(\boldsymbol{x}, z)B(\boldsymbol{x}', z')] = \gamma(\boldsymbol{x} - \boldsymbol{x}')\frac{c_\alpha}{2H(2H-1)}\big(z^{2H} + z'^{2H} - |z - z'|^{2H}\big).$$

In this case the stochastic integral in (6) can be understood as a generalized Stieljes integral (as $H > 1/2$).

3 Statistics of the wave field

In this section we describe how to compute the moments of the wave field. By Itô's formula and (6), the coherent (or mean) wave satisfies the Schrödinger equation with homogeneous damping (for $z > 0$):

$$\partial_z \mathbb{E}[\hat{\phi}] = \frac{ic_o}{2\omega}\Delta_\perp \mathbb{E}[\hat{\phi}] - \frac{\omega^2 \gamma(\mathbf{0})}{8c_o^2}\mathbb{E}[\hat{\phi}], \tag{8}$$

and therefore $\mathbb{E}\big[\hat{\phi}(\boldsymbol{x}, z)\big] = \hat{\phi}_0(\boldsymbol{x}, z)\exp(-z/Z_{\rm sca})$, where $\hat{\phi}_0$ is the solution in the homogeneous medium. The coherent wave amplitude decays exponentially with the propagation distance and the characteristic decay length is the *scattering mean free path* $Z_{\rm sca}$:

$$Z_{\rm sca} = \frac{8c_o^2}{\gamma(\mathbf{0})\omega^2}. \tag{9}$$

This result shows that any coherent imaging or communication method

fails in random media when the propagation distance is larger than the scattering mean free path [23].

The mean Wigner distribution defined by

$$W_{\rm m}(\boldsymbol{x}, \boldsymbol{\xi}, z) = \int_{\mathbb{R}^2} \exp\big(-i\boldsymbol{\xi}\cdot\boldsymbol{y}\big)\mathbb{E}\left[\hat{\phi}\big(\boldsymbol{x} + \frac{\boldsymbol{y}}{2}, z\big)\overline{\hat{\phi}}\big(\boldsymbol{x} - \frac{\boldsymbol{y}}{2}, z\big)\right] \mathrm{d}\boldsymbol{y} \tag{10}$$

is the angularly-resolved mean wave energy density (the bar stands for complex conjugation). By Itô's formula and (6), it solves the *radiative transport equation*

$$\partial_z W_{\rm m} + \frac{c_o}{\omega}\boldsymbol{\xi}\cdot\nabla_{\boldsymbol{x}} W_{\rm m} = \frac{\omega^2}{4(2\pi)^2 c_o^2}\int_{\mathbb{R}^2} \hat{\gamma}(\boldsymbol{\kappa})\big[W_{\rm m}(\boldsymbol{\xi}-\boldsymbol{\kappa}) - W_{\rm m}(\boldsymbol{\xi})\big]\mathrm{d}\boldsymbol{\kappa}, \tag{11}$$

starting from $W_{\rm m}(\boldsymbol{x}, \boldsymbol{\xi}, z=0) = W_0(\boldsymbol{x}, \boldsymbol{\xi})$, the Wigner distribution of the initial field f. $\hat{\gamma}$ is the Fourier transform of γ and determines the scattering cross section of the radiative transport equation. This result shows that the fields observed at nearby points are correlated and their correlations contain information about the medium. Accordingly, one should use local cross correlations for imaging and communication in random media [7, 9].

In order to quantify the stability of correlation-based imaging methods, one needs to evaluate variances of empirical correlations, which involves the fourth-order moment:

$$\begin{aligned} M_4(\boldsymbol{q}_1, \boldsymbol{q}_2, \boldsymbol{r}_1, \boldsymbol{r}_2, z) = \mathbb{E}\Big[&\hat{\phi}\big(\frac{\boldsymbol{r}_1 + \boldsymbol{r}_2 + \boldsymbol{q}_1 + \boldsymbol{q}_2}{2}, z\big)\hat{\phi}\big(\frac{\boldsymbol{r}_1 - \boldsymbol{r}_2 + \boldsymbol{q}_1 - \boldsymbol{q}_2}{2}, z\big) \\ &\times\overline{\hat{\phi}}\big(\frac{\boldsymbol{r}_1 + \boldsymbol{r}_2 - \boldsymbol{q}_1 - \boldsymbol{q}_2}{2}, z\big)\overline{\hat{\phi}}\big(\frac{\boldsymbol{r}_1 - \boldsymbol{r}_2 - \boldsymbol{q}_1 + \boldsymbol{q}_2}{2}, z\big)\Big]. \end{aligned} \tag{12}$$

By Itô's formula and (6), it satisfies the Schrödinger-type equation

$$\partial_z M_4 = \frac{ic_o}{\omega}\big(\nabla_{\boldsymbol{r}_1}\cdot\nabla_{\boldsymbol{q}_1} + \nabla_{\boldsymbol{r}_2}\cdot\nabla_{\boldsymbol{q}_2}\big)M_4 + \frac{\omega^2}{4c_o^2}U_4(\boldsymbol{q}_1, \boldsymbol{q}_2, \boldsymbol{r}_1, \boldsymbol{r}_2)M_4, \tag{13}$$

with the generalized potential

$$\begin{aligned} U_4(\boldsymbol{q}_1, \boldsymbol{q}_2, \boldsymbol{r}_1, \boldsymbol{r}_2) = &\gamma(\boldsymbol{q}_2 + \boldsymbol{q}_1) + \gamma(\boldsymbol{q}_2 - \boldsymbol{q}_1) + \gamma(\boldsymbol{r}_2 + \boldsymbol{q}_1) + \gamma(\boldsymbol{r}_2 - \boldsymbol{q}_1) \\ &- \gamma(\boldsymbol{q}_2 + \boldsymbol{r}_2) - \gamma(\boldsymbol{q}_2 - \boldsymbol{r}_2) - 2\gamma(\mathbf{0}). \end{aligned} \tag{14}$$

These moment equations have been known for a long time [33]. Recently it was shown [28] that in the regime "$\lambda \ll \ell_c \ll r_o \ll z$" the fourth-order moment can be expressed explicitly in terms of the function γ. These results can be used to address a wide range of applications in imaging and communication.

4 The scintillation index

In this section we study the intensity fluctuations of the wave field solution of (6) and characterize the scintillation index which quantifies the relative intensity fluctuations. It is a fundamental quantity associated for instance with light propagation through the atmosphere [33]. It is defined as the square coefficient of variation of the intensity [33, Eq. (20.151)]:

$$S(\boldsymbol{x}, z) = \frac{\mathbb{E}\big[\big|\hat{\phi}(\boldsymbol{x}, z)\big|^4\big] - \mathbb{E}\big[\big|\hat{\phi}(\boldsymbol{x}, z)\big|^2\big]^2}{\mathbb{E}\big[\big|\hat{\phi}(\boldsymbol{x}, z)\big|^2\big]^2}. \tag{15}$$

When the spatial profile of the source (or the initial beam) has a Gaussian profile,

$$f(\boldsymbol{x}) = \exp\Big(-\frac{|\boldsymbol{x}|^2}{r_o^2}\Big), \tag{16}$$

and when "$\lambda \ll \ell_c \ll r_o \ll z$", the behavior of the scintillation index can be described as follows [28].

Proposition 4.1. *Let us consider the following form of the covariance function of the medium fluctuations:*

$$\gamma(\boldsymbol{x}) = \gamma(\mathbf{0})\tilde{\gamma}\Big(\frac{\boldsymbol{x}}{\ell_{\rm c}}\Big),$$

with $\tilde{\gamma}(\mathbf{0}) = 1$ and the width of the function $\tilde{\gamma}$ is of order one. In the regime "$\lambda \ll \ell_c \ll r_o \ll z$" the scintillation index (15) has the following expression:

$$S(\boldsymbol{x}, z) = 1 - \frac{\exp\Big(-\frac{2|\boldsymbol{x}|^2}{r_o^2}\Big)}{\Big|\frac{1}{4\pi}\int_{\mathbb{R}^2} \exp\Big(\frac{2z}{Z_{\rm sca}}\int_0^1 \tilde{\gamma}\big(\boldsymbol{v}\frac{z}{Z_{\rm c}}s\big)\mathrm{d}s - \frac{|\boldsymbol{v}|^2}{4} + i\boldsymbol{v}\cdot\frac{\boldsymbol{x}}{r_o}\Big)\mathrm{d}\boldsymbol{v}\Big|^2}. \tag{17}$$

In fact this result follows from the complete expressions of the second moment of the intensity and the second moment of the field that are given in [28]. The scintillation index at the beam center $\boldsymbol{x} = \mathbf{0}$ is a function of $z/Z_{\rm sca}$ and $z/Z_{\rm c}$ only, where $Z_{\rm c} = \omega r_o \ell_{\rm c}/c_o$ is the typical propagation distance for which diffractive effects are of order one, as shown in [25, Eq. (4.4)]. It is interesting to note that, even if the propagation distance is larger than the scattering mean free path, the scintillation index can be smaller than one if $Z_{\rm c}$ is small compared to $Z_{\rm sca}$.

In order to get more explicit expressions that facilitate interpretation of the results let us assume that $\gamma(\boldsymbol{x})$ is smooth and can be expanded as

$$\gamma(\boldsymbol{x}) = \gamma(\mathbf{0})\Big(1 - \frac{|\boldsymbol{x}|^2}{\ell_{\rm c}^2} + o\big(\frac{|\boldsymbol{x}|^2}{\ell_{\rm c}^2}\big)\Big), \qquad \boldsymbol{x} \to \mathbf{0}. \tag{18}$$

When scattering is strong in the sense that the propagation distance is larger than the scattering mean free path $z \gg Z_{\rm sca}$, the expressions of the second moments of the field and of the intensity can be simplified:

$$\Gamma^{(2)}(\boldsymbol{x},\boldsymbol{y},z) := \mathbb{E}\Big[\hat{\phi}\big(\boldsymbol{x}+\frac{\boldsymbol{y}}{2},z\big)\overline{\hat{\phi}}\big(\boldsymbol{x}-\frac{\boldsymbol{y}}{2},z\big)\Big] = \frac{r_o^2}{R_z^2}\exp\Big(-\frac{|\boldsymbol{x}|^2}{R_z^2}-\frac{|\boldsymbol{y}|^2}{\rho_z^2}+i\frac{\omega\gamma(\boldsymbol{0})z^2\boldsymbol{x}\cdot\boldsymbol{y}}{2c_o\ell_{\rm c}^2R_z^2}\Big),$$
$$\Gamma^{(4)}(\boldsymbol{x},\boldsymbol{y},z) := \mathbb{E}\Big[\big|\hat{\phi}\big(\boldsymbol{x}+\frac{\boldsymbol{y}}{2},z\big)\big|^2\big|\hat{\phi}\big(\boldsymbol{x}-\frac{\boldsymbol{y}}{2},z\big)\big|^2\Big] = |\Gamma^{(2)}(\boldsymbol{x},\boldsymbol{0},z)|^2+|\Gamma^{(2)}(\boldsymbol{x},\boldsymbol{y},z)|^2,$$

where the beam radius R_z is

$$R_z^2 = r_o^2+\frac{\gamma(\boldsymbol{0})z^3}{3\ell_{\rm c}^2} \tag{19}$$

and the correlation radius of the beam ρ_z is

$$\rho_z^2 = \frac{4c_o^2\ell_{\rm c}^2}{\omega^2\gamma(\boldsymbol{0})z}\frac{r_o^2+\frac{\gamma(\boldsymbol{0})z^3}{3\ell_{\rm c}^2}}{r_o^2+\frac{\gamma(\boldsymbol{0})z^3}{12\ell_{\rm c}^2}}. \tag{20}$$

Note that the fourth-order moments satisfy the Isserlis formula (i.e. they can be expressed in terms of sums of products of second-order moments), and therefore the scintillation index $S(\boldsymbol{x},z)$ is equal to one. This observation is consistent with the physical intuition that, in the strongly scattering regime $z/Z_{\rm sca} \gg 1$, the wave field is conjectured to have zero-mean complex circularly symmetric Gaussian statistics, and therefore the intensity is expected to have exponential (or Rayleigh) distribution [14, 33].

5 Fluctuations of the Wigner distribution

In this section we give an explicit characterization of the signal-to-noise ratio of the Wigner distribution. The Wigner distribution of the wave field is defined by

$$W(\boldsymbol{x},\boldsymbol{\xi},z) = \int_{\mathbb{R}^2}\exp\big(-i\boldsymbol{\xi}\cdot\boldsymbol{y}\big)\hat{\phi}\big(\boldsymbol{x}+\frac{\boldsymbol{y}}{2},z\big)\overline{\hat{\phi}}\big(\boldsymbol{x}-\frac{\boldsymbol{y}}{2},z\big)\mathrm{d}\boldsymbol{y}. \tag{21}$$

It can be interpreted as the angularly-resolved wave energy density (note, however, that it is real-valued but not always non-negative valued). Its expectation satisfies the radiative transport equation (11). It is known that the Wigner distribution is not statistically stable, and that it is necessary to smooth it (that is to say, to convolve it with a smoothing kernel) to get a quantity that can be measured in a statistically stable way (that is to say, the smoothed Wigner distribution for one typical realization is approximately equal to its expected value) [3, 44]. Our goal in this section is to quantify this statistical stability.

Let us consider two positive parameters $r_{\rm s}$ and $\xi_{\rm s}$ and define the smoothed Wigner distribution:

$$W_{\rm s}(\boldsymbol{x},\boldsymbol{\xi},z) = \frac{1}{(2\pi)^2r_{\rm s}^2\xi_{\rm s}^2}\iint_{\mathbb{R}^4}W(\boldsymbol{x}-\boldsymbol{x}',\boldsymbol{\xi}-\boldsymbol{\xi}',z)\exp\Big(-\frac{|\boldsymbol{x}'|^2}{2r_{\rm s}^2}-\frac{|\boldsymbol{\xi}'|^2}{2\xi_{\rm s}^2}\Big)\mathrm{d}\boldsymbol{x}'\mathrm{d}\boldsymbol{\xi}'. \tag{22}$$

If we denote by ρ_z the correlation radius of the field (given by (20) in the strongly scattering regime), we may anticipate that $r_{\rm s}$ and $1/\xi_{\rm s}$ should be of the order of ρ_z to ensure averaging.

The coefficient of variation $C_{\rm s}$ of the smoothed Wigner distribution, which characterizes its statistical stability, is defined by:

$$C_{\rm s}(\boldsymbol{x},\boldsymbol{\xi},z)=\frac{\sqrt{\mathbb{E}[W_{\rm s}(\boldsymbol{x},\boldsymbol{\xi},z)^2]-\mathbb{E}[W_{\rm s}(\boldsymbol{x},\boldsymbol{\xi},z)]^2}}{\mathbb{E}[W_{\rm s}(\boldsymbol{x},\boldsymbol{\xi},z)]}. \tag{23}$$

An exact expression of the coefficient of variation of the smoothed Wigner distribution can be derived in the regime "$\lambda \ll \ell_c \ll r_o \ll z$" [28]. It involves four-dimensional integrals and it is complicated to interpret it. This expression becomes simple in the strongly scattering regime $z \gg Z_{\rm sca}$. We then get the following expression for the coefficient of variation [28].

Proposition 5.1. *In the regime "$\lambda \ll \ell_c \ll r_o \ll z$", if additionally $z \gg Z_{\rm sca}$ and γ can be expanded as (18), then the coefficient of variation of the smoothed Wigner distribution (22) satisfies:*

$$C_{\rm s}(\boldsymbol{x},\boldsymbol{\xi},z)^2=\frac{\frac{1}{\xi_{\rm s}^2\rho_z^2}+1}{\frac{4r_{\rm s}^2}{\rho_z^2}+1}, \tag{24}$$

where ρ_z is the correlation radius (20).

Note that the coefficient of variation becomes independent of $\boldsymbol{x}$ and $\boldsymbol{\xi}$. Eq. (24) is a simple enough formula to help determining the smoothing parameters $\xi_{\rm s}$ and $r_{\rm s}$ that are needed to reach a given value for the coefficient of variation:

- For $2\xi_{\rm s}r_{\rm s}=1$, we have $C_{\rm s}(\boldsymbol{x},\boldsymbol{\xi},z)=1$.
- For $2\xi_{\rm s}r_{\rm s}<1$ (resp. >1) we have $C_{\rm s}(\boldsymbol{x},\boldsymbol{\xi},z)>1$ (resp. <1); in other words, the smoothed Wigner transform can be considered as statistically stable as soon as $2\xi_{\rm s}r_{\rm s}>1$.

The critical value $r_{\rm s}=1/(2\xi_{\rm s})$ is indeed special. In this case, the smoothed Wigner distribution (22) can be written as the double convolution of the Wigner distribution W of the random field $\hat{\phi}(\cdot,z)$ (defined by (21)) with the Wigner distribution

$$W_{\rm g}(\boldsymbol{x},\boldsymbol{\xi})=\int_{\mathbb{R}^2}\exp\big(-i\boldsymbol{\xi}\cdot\boldsymbol{y}\big)\hat{\phi}_{\rm g}\big(\boldsymbol{x}+\frac{\boldsymbol{y}}{2}\big)\overline{\hat{\phi}_{\rm g}}\big(\boldsymbol{x}-\frac{\boldsymbol{y}}{2}\big){\rm d}\boldsymbol{y} \tag{25}$$

of the Gaussian state

$$\hat{\phi}_{\rm g}(\boldsymbol{x})=\exp\big(-\xi_{\rm s}^2|\boldsymbol{x}|^2\big), \tag{26}$$

since we have

$$W_{\rm g}(\boldsymbol{x},\boldsymbol{\xi})=\frac{2\pi}{\xi_{\rm s}^2}\exp\Big(-2\xi_{\rm s}^2|\boldsymbol{x}|^2-\frac{|\boldsymbol{\xi}|^2}{2\xi_{\rm s}^2}\Big),$$

and therefore

$$W_{\rm s}(\boldsymbol{x},\boldsymbol{\xi},z)=\frac{4\xi_{\rm s}^2}{(2\pi)^3}\iint_{\mathbb{R}^4}W(\boldsymbol{x}-\boldsymbol{x}',\boldsymbol{\xi}-\boldsymbol{\xi}',z)W_{\rm g}(\boldsymbol{x}',\boldsymbol{\xi}'){\rm d}\boldsymbol{x}'{\rm d}\boldsymbol{\xi}', \tag{27}$$

for $r_s = 1/(2\xi_s)$. It is known that the convolution of a Wigner distribution with a kernel that is itself the Wigner distribution of a function (such as W_g) is nonnegative real valued (the smoothed Wigner distribution obtained with the Gaussian W_g is called Husimi function) [10, 39]. This can be shown easily in our case as the smoothed Wigner distribution can be written as

$$W_s(\boldsymbol{x}, \boldsymbol{\xi}, z) = \frac{2\xi_s^2}{\pi} \Big| \int_{\mathbb{R}^2} \exp\big(i\boldsymbol{\xi} \cdot \boldsymbol{x}'\big) \overline{\hat{\phi}_g}(\boldsymbol{x}') \hat{\phi}(\boldsymbol{x} - \boldsymbol{x}', z) \mathrm{d}\boldsymbol{x}' \Big|^2, \tag{28}$$

for $r_s = 1/(2\xi_s)$. From this representation formula of W_s valid for $r_s = 1/(2\xi_s)$, we can see that it is the square modulus of a linear functional of $\hat{\phi}(\cdot, z)$. The physical intuition that $\hat{\phi}(\cdot, z)$ has circularly symmetric complex Gaussian statistics in strongly scattering media then predicts that $W_s(\boldsymbol{x}, \boldsymbol{\xi}, z)$ should have an exponential distribution, because the sum of the squares of two independent real-valued Gaussian random variables has an exponential distribution. This is indeed consistent with our theoretical finding that $C_s = 1$ for $r_s = 1/(2\xi_s)$.

If $r_s > 1/(2\xi_s)$, by observing that

$$\exp\Big(-\frac{|\boldsymbol{x}|^2}{2r_s^2}\Big) = \int_{\mathbb{R}^2} \Psi(\boldsymbol{x} - \boldsymbol{x}') \exp\big(-2\xi_s^2 |\boldsymbol{x}'|^2\big) \mathrm{d}\boldsymbol{x}',$$

where the function Ψ is defined by

$$\Psi(\boldsymbol{x}) = \frac{8\xi_s^4 r_s^2}{\pi(4\xi_s^2 r_s^2 - 1)} \exp\Big(-\frac{2\xi_s^2 |\boldsymbol{x}|^2}{(4\xi_s^2 r_s^2 - 1)}\Big), \tag{29}$$

we find that the smoothed Wigner distribution (22) can be expressed as:

$$W_s(z, \boldsymbol{x}, \boldsymbol{\xi}) = \int_{\mathbb{R}^2} \Psi(\boldsymbol{x} - \boldsymbol{x}') \left(\frac{2\xi_s^2}{\pi} \Big| \int_{\mathbb{R}^2} \exp\big(i\boldsymbol{\xi} \cdot \boldsymbol{x}''\big) \overline{\hat{\phi}_g}(\boldsymbol{x}'') \hat{\phi}(\boldsymbol{x}' - \boldsymbol{x}'', z) \mathrm{d}\boldsymbol{x}'' \Big|^2 \right) \mathrm{d}\boldsymbol{x}', \tag{30}$$

for $r_s > 1/(2\xi_s)$. From this representation formula for W_s valid for $r_s > 1/(2\xi_s)$, we can see that it is nonnegative valued and that it is a local average of (28), which has a unit coefficient of variation in the strongly scattering regime. That is why the coefficient of variation of the smoothed Wigner distribution is smaller than one when $r_s > 1/(2\xi_s)$.

6 Green's function estimation with noise sources

The previous section has explained that the cross correlation of the wave field (or equivalently the Wigner distribution which is its local Fourier transform) is a convenient way to look at waves propagating in complex media. In this section we show that it is also useful to study waves emitted by unknown noise sources. In Section 7 we will combine both situations and show that incoherent illumination can provide new paradigms and offer new opportunities for imaging in complex media.

We aim to exhibit a relation between the cross correlation of the signals emitted by noise sources and recorded by two sensors and the Green's function between the sensors.

The Green's function is the signal recorded by the second sensor when the first one transmits a short (Dirac) pulse. The relation between the cross correlation of the recorded noise signals and the Green's function is very important. Indeed, in standard imaging, an array of sources transmits waves that are recorded by an array of receivers, that can be collocated with the array of sources (called an active array). One then gets the matrix of Green's functions from the sources to the receivers, that can be processed for imaging purposes. In ambient noise imaging, an array of receivers (called a passive array) records the waves emitted by ambient noise sources. Under favorable circumstances, the matrix of cross correlations of the signals recorded by the receivers gives the matrix of Green's functions between the receivers. In other words, the passive array data has been transformed into an active array data ! The fact that ambient noise illumination allows for Green's function estimation and subsequent imaging opens fascinating perspectives. In seismology, it means that information is present in the seismic noise recorded by networks of seismometers and that it can be extracted by computing cross correlations.

We consider the solution u of the scalar wave equation in a three-dimensional inhomogeneous medium with propagation speed $c(\vec{\boldsymbol{x}})$:

$$\frac{1}{c^2(\vec{\boldsymbol{x}})}\frac{\partial^2 u}{\partial t^2} - \Delta_{\vec{\boldsymbol{x}}} u = n(t, \vec{\boldsymbol{x}}). \tag{31}$$

The term $n(t, \vec{\boldsymbol{x}})$ models noise sources. It is a zero-mean stationary (in time) random process with autocorrelation function

$$\langle n(t_1, \vec{\boldsymbol{y}}_1) n(t_2, \vec{\boldsymbol{y}}_2)\rangle = F(t_2 - t_1)\Gamma(\vec{\boldsymbol{y}}_1, \vec{\boldsymbol{y}}_2). \tag{32}$$

Here $\langle\cdot\rangle$ stands for statistical average with respect to the distribution of the noise sources.

The time distribution of the noise sources is characterized by the correlation function $F(t_2 - t_1)$, which is a function of $t_2 - t_1$ only because of time stationarity. The Fourier transform $\hat{F}(\omega)$ of the time correlation function $F(t)$ is a nonnegative, even, real-valued function proportional to the power spectral density of the sources:

$$\hat{F}(\omega) = \int_{\mathbb{R}} F(t) e^{i\omega t} \mathrm{d}t. \tag{33}$$

The spatial distribution of the noise sources is characterized by the autocovariance function $\Gamma(\vec{\boldsymbol{y}}_1, \vec{\boldsymbol{y}}_2)$. In this review paper we assume that the random process n is delta-correlated in space:

$$\Gamma(\vec{\boldsymbol{y}}_1, \vec{\boldsymbol{y}}_2) = K(\vec{\boldsymbol{y}}_1)\delta(\vec{\boldsymbol{y}}_1 - \vec{\boldsymbol{y}}_2), \tag{34}$$

although it is possible to address correlated noise sources, as shown in [5, 22]. The nonnegative valued function K characterizes the spatial support of the sources.

The solution of the wave equation (31) has the integral representation:

$$u(t, \vec{\boldsymbol{x}}) = \int_{\mathbb{R}^3}\int_{\mathbb{R}} n(t - s, \vec{\boldsymbol{y}}) G(s, \vec{\boldsymbol{x}}, \vec{\boldsymbol{y}}) \mathrm{d}s \mathrm{d}\vec{\boldsymbol{y}},$$

where $G(t, \vec{\boldsymbol{x}}, \vec{\boldsymbol{y}})$ is the time-dependent Green's function, that is to say, the fundamental solution of the three-dimensional scalar wave equation:

$$\frac{1}{c^2(\vec{\boldsymbol{x}})}\frac{\partial^2 G}{\partial t^2} - \Delta_{\vec{\boldsymbol{x}}} G = \delta(t)\delta(\vec{\boldsymbol{x}} - \vec{\boldsymbol{y}}).$$

The empirical cross correlation of the signals recorded at $\vec{\boldsymbol{x}}_1$ and $\vec{\boldsymbol{x}}_2$ for an integration time T is

$$C_T(\tau, \vec{\boldsymbol{x}}_1, \vec{\boldsymbol{x}}_2) = \frac{1}{T}\int_0^T u(t, \vec{\boldsymbol{x}}_1)u(t+\tau, \vec{\boldsymbol{x}}_2)\mathrm{d}t. \tag{35}$$

It is a statistically stable quantity, in the sense that for a large integration time T, the empirical cross correlation C_T is independent of the realization of the noise sources and it is equal to its expectation. This is stated in the following proposition [21].

Proposition 6.1. *1. The expectation of the empirical cross correlation C_T (with respect to the statistics or distribution of the sources) is independent of T:*

$$\langle C_T(\tau, \vec{\boldsymbol{x}}_1, \vec{\boldsymbol{x}}_2)\rangle = C^{(1)}(\tau, \vec{\boldsymbol{x}}_1, \vec{\boldsymbol{x}}_2), \tag{36}$$

where the statistical cross correlation $C^{(1)}$ is given by

$$C^{(1)}(\tau, \vec{\boldsymbol{x}}_1, \vec{\boldsymbol{x}}_2) = \frac{1}{2\pi}\int_{\mathbb{R}^3}\int_{\mathbb{R}} \hat{F}(\omega)K(\vec{\boldsymbol{y}})\overline{\hat{G}(\omega, \vec{\boldsymbol{x}}_1, \vec{\boldsymbol{y}})}\hat{G}(\omega, \vec{\boldsymbol{x}}_2, \vec{\boldsymbol{y}})e^{-i\omega\tau}\mathrm{d}\omega\mathrm{d}\vec{\boldsymbol{y}}, \tag{37}$$

and $\hat{G}(\omega, \vec{\boldsymbol{x}}, \vec{\boldsymbol{y}})$ is the time-harmonic Green's function (i.e. the Fourier transform of $G(t, \vec{\boldsymbol{x}}, \vec{\boldsymbol{y}})$).

2. The empirical cross correlation C_T is a self-averaging quantity:

$$C_T(\tau, \vec{\boldsymbol{x}}_1, \vec{\boldsymbol{x}}_2) \overset{T\to\infty}{\longrightarrow} C^{(1)}(\tau, \vec{\boldsymbol{x}}_1, \vec{\boldsymbol{x}}_2), \tag{38}$$

in probability (with respect to the distribution of the sources).

Eq. (37) holds whatever the spatial support of the sources but it does not give a simple relation between the cross correlation of the recorded noise signals and the Green's function. Such a relation emerges when the spatial support of the sources is extended. We give below a simple statement when the noise sources are located on the surface of a ball that encloses both the inhomogeneous region and the sensors, located at $\vec{\boldsymbol{x}}_1$ and $\vec{\boldsymbol{x}}_2$.

Proposition 6.2. *We assume that the medium is homogeneous outside the ball $B(\mathbf{0}, D)$ with center $\mathbf{0}$ and radius D, and that the sources are localized with a uniform density on the surface of the sphere $\partial B(\mathbf{0}, L)$ with center $\mathbf{0}$ and radius L. If $L \gg D$, then for any $\vec{\boldsymbol{x}}_1, \vec{\boldsymbol{x}}_2 \in B(\mathbf{0}, D)$, we have*

$$\frac{\partial}{\partial\tau}C^{(1)}(\tau, \vec{\boldsymbol{x}}_1, \vec{\boldsymbol{x}}_2) = -\frac{c_o}{2}\left[F * G(\tau, \vec{\boldsymbol{x}}_1, \vec{\boldsymbol{x}}_2) - F * G(-\tau, \vec{\boldsymbol{x}}_1, \vec{\boldsymbol{x}}_2)\right]. \tag{39}$$

Proposition 6.2 can be found in [48, 60]. The proof is based on the Helmholtz-Kirchhoff identity, which results from the second Green's identity and the Sommerfeld radiation condition. It is simple and gives the desired result quickly, but it requires a full aperture illumination. Multiscale analysis reveals that full aperture illumination is sufficient but not necessary for the cross correlation to be related to the Green's function [23].

Proposition 6.2 shows that, when the noise sources surround the region of interest, then the lag-time derivative of the cross correlation of the signals recorded at two observation points is the Green's function between these two points, up to a convolution (in time) with

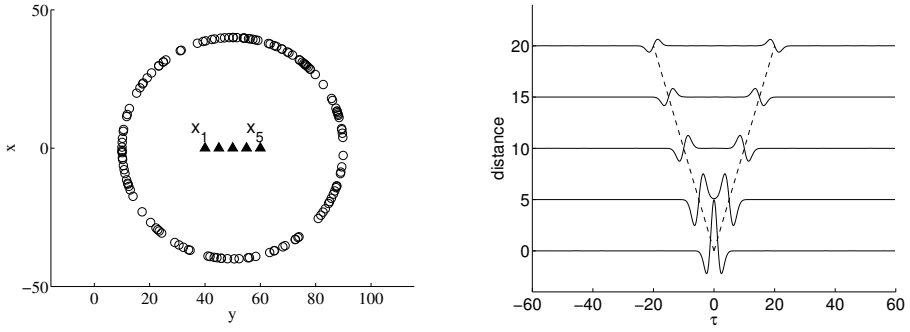

a) Configuration **b)** $C^{(1)}(\tau, \vec{\boldsymbol{x}}_1, \vec{\boldsymbol{x}}_j)$

Figure 1: The configuration is shown in the plane (xy) in Figure a: the circles are the noise sources and the triangles are the sensors (the distance between two successive sensors is 5). The sources are randomly distributed on the surface of the three-dimensional sphere with center at $(0, 50, 0)$ and radius 40. Figure b shows the cross correlation $\tau \to C^{(1)}(\tau, \vec{\boldsymbol{x}}_1, \vec{\boldsymbol{x}}_j)$ between the pairs of sensors $(\vec{\boldsymbol{x}}_1, \vec{\boldsymbol{x}}_j)$, $j = 1, \ldots, 5$, versus the distance $|\vec{\boldsymbol{x}}_j - \vec{\boldsymbol{x}}_1|$. For $j \geq 2$ the values have been multiplied by 6 as the autocorrelation function $(j = 1)$ takes larger values than the cross correlation functions $(j \geq 2)$. Here $c_o = 1$.

the time covariance function of the noise sources and a symmetrization (which means that we get in fact the causal and the anti-causal Green's functions). We can present an illustration of this result when the medium is homogeneous with background velocity c_o and the Green's function is $G(t, \vec{\boldsymbol{x}}, \boldsymbol{y}) = \frac{1}{4\pi|\vec{\boldsymbol{x}}-\vec{\boldsymbol{y}}|}\delta(t - \frac{|\vec{\boldsymbol{x}}-\vec{\boldsymbol{y}}|}{c_o})$. If $F(t) = -g''(t)$ with $g(t) = \exp(-t^2/4)$ (the prime stands for derivative), so that $\hat{F}(\omega) = 2\sqrt{\pi}\omega^2 \exp(-\omega^2)$, then the cross correlation is by (39):

$$C^{(1)}(\tau, \vec{\boldsymbol{x}}_1, \vec{\boldsymbol{x}}_2) = \frac{c_o}{8\pi|\vec{\boldsymbol{x}}_1 - \vec{\boldsymbol{x}}_2|}\left[g'\Big(\tau - \frac{|\vec{\boldsymbol{x}}_1 - \vec{\boldsymbol{x}}_2|}{c_o}\Big) - g'\Big(\tau + \frac{|\vec{\boldsymbol{x}}_1 - \vec{\boldsymbol{x}}_2|}{c_o}\Big)\right].$$

The autocorrelation function is

$$C^{(1)}(\tau, \vec{\boldsymbol{x}}_1, \vec{\boldsymbol{x}}_1) = -\frac{1}{4\pi}g''(\tau)\,.$$

These two functions can be seen in Figure 1: the autocorrelation function $C^{(1)}(\tau, \vec{\boldsymbol{x}}_1, \vec{\boldsymbol{x}}_1)$ has the form of the second derivative of a Gaussian function, and the cross correlation $C^{(1)}(\tau, \vec{\boldsymbol{x}}_1, \vec{\boldsymbol{x}}_j)$, $j \geq 2$, has two symmetric peaks with the form of the first derivative of a Gaussian function and centered at the travel times $\pm|\vec{\boldsymbol{x}}_1 - \vec{\boldsymbol{x}}_j|/c_o$. From the imaging point of view, this means that the travel times between the sensors can be estimated from the cross correlations of the noise signals and subsequently background velocity estimation can be carried out tomographically.

7 An example of incoherent wave imaging in complex media: Ghost imaging

In this section we study an imaging method called ghost imaging introduced in the optics literature. It illustrates the fact that incoherent illumination can be beneficial for correlation-based imaging in complex media. The experimental set-up proposed in [57, 50] is plotted in Figure 2. The waves are emitted by a noise (or partially coherent) source. A beam splitter is used to generate two wave beams from this source:
- the "reference beam", labeled ①, propagates through a homogeneous or scattering medium up to a high-resolution detector that measures the spatially resolved transmitted intensity.
- the "signal beam", labeled ②, propagates through a homogeneous or scattering medium and interacts with an object to be imaged. The total transmitted intensity is measured by a bucket detector that measures the spatially integrated transmitted intensity.
This method is called ghost imaging because the high-resolution detector does not see the object to be imaged, and nevertheless a high-resolution image of the object is obtained by cross-correlating the two measured intensity signals. From the previous section we can anticipate that something may indeed happen when cross correlating these signals because the cross correlation should be related to the Green's function between the plane of the high-resolution detector in reference path ① (or the corresponding plane just before the object in the signal path ②) and the plane of the bucket detector in ②. The relation is not, however, clear when only spatially-integrated intensities are measured, which requires a detailed analysis.

The object to be imaged is a mask modeled by a transmission function $\mathcal{T}(\boldsymbol{x})$. In the experiments, the object is typically a double slit [50]. The source is located in the plane $z = 0$. The propagation distance from the source to the high-resolution detector in the reference path ① is L. The propagation distance from the source to the object in the signal path ② is L as well, and the propagation distance from the object to the bucket detector is L_0. In each path the scalar wave $(t, \vec{\boldsymbol{x}}) \mapsto u_j(t, \vec{\boldsymbol{x}})$, $j = 1, 2$, satisfies the scalar wave equation:

$$\frac{1}{c_j(\vec{\boldsymbol{x}})^2}\frac{\partial^2 u_j}{\partial t^2} - \Delta_{\vec{\boldsymbol{x}}} u_j = n(t, \boldsymbol{x})\delta(z), \tag{40}$$

where $c_j(\vec{\boldsymbol{x}})$ is the speed of propagation in the medium corresponding to the jth path and the forcing term $(t, \boldsymbol{x}) \mapsto n(t, \boldsymbol{x})$ models the source (identical for the two waves).

In the ghost experiment the source is typically a laser beam passed through a rotating glass diffuser [57, 50]. We model it as

$$n(t, \boldsymbol{x}) = f(t, \boldsymbol{x})e^{-i\omega_o t} + c.c., \tag{41}$$

where $c.c.$ stands for complex conjugate, ω_o is the carrier frequency, and $f(t, \boldsymbol{x})$ is the complex-valued slowly varying envelope, whose Fourier transform (in time) has a typical width that is much smaller than ω_o. It is assumed to be a complex-valued, zero-mean stationary Gaussian process with the covariance function:

$$\langle f(t, \boldsymbol{x})\overline{f(t', \boldsymbol{x}')}\rangle = F(t - t')\Gamma(\boldsymbol{x}, \boldsymbol{x}'), \tag{42}$$

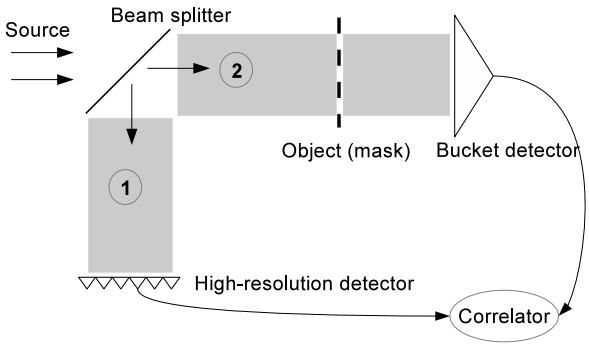

Figure 2: The ghost imaging setup. A partially coherent source is split into two beams by a beam splitter. The reference beam (labeled ①) does not interact with the object and its intensity is measured by a high-resolution detector. The signal beam (labeled ②) interacts with the object to be imaged and its intensity is measured by a bucket (single-pixel) detector. From [20].

with $F(0) = 1$ (with real-valued functions F and Γ). The width of the Fourier transform of F is much smaller than ω_o. Note that the modeling is similar to the one used for correlation-based imaging using ambient noise sources as discussed in the previous section. In this framework the scalar wave fields u_j, $j = 1, 2$, can be written in the form

$$u_j(t, \vec{\boldsymbol{x}}) = v_j(t, \vec{\boldsymbol{x}})e^{-i\omega_o t} + c.c..$$

The detectors measure the intensities, i.e. the square moduli of the slowly varying envelopes v_j, $j = 1, 2$. More exactly, the quantity that is measured by the high-resolution detector is the spatially-resolved intensity in the plane $z = L$ of the reference path ①:

$$I_1(t, \boldsymbol{x}) = \big|v_1\big(t, (\boldsymbol{x}, L)\big)\big|^2. \tag{43}$$

The quantity that is measured by the bucket detector is the spatially-integrated intensity in the plane $z = L + L_0$ of the signal path ②:

$$I_2(t) = \int_{\mathbb{R}^2} \big|v_2\big(t, (\boldsymbol{x}, L + L_0)\big)\big|^2 \mathrm{d}\boldsymbol{x}. \tag{44}$$

These two quantities are correlated and their cross correlation defines the ghost imaging function:

$$\mathcal{C}_T(\boldsymbol{x}) = \frac{1}{T}\int_0^T I_1(t, \boldsymbol{x})I_2(t)\mathrm{d}t - \Big[\frac{1}{T}\int_0^T I_1(t, \boldsymbol{x})\mathrm{d}t\Big]\Big[\frac{1}{T}\int_0^T I_2(t)\mathrm{d}t\Big]. \tag{45}$$

We consider the partially coherent case:

$$\Gamma(\boldsymbol{x}, \boldsymbol{x}') = I_o \exp\Big(-\frac{|\boldsymbol{x} + \boldsymbol{x}'|^2}{2r_o^2} - \frac{|\boldsymbol{x} - \boldsymbol{x}'|^2}{2\rho_o^2}\Big), \tag{46}$$

in which the source is assumed to have a spatial support in the form of a Gaussian with radius r_o and a local Gaussian correlation function with radius ρ_o. This model is called Gaussian-Schell in the optics literature [38]. Note that we always have $r_o \geq \rho_o$ (because Γ is a positive kernel). The limit case $\rho_o \to 0$ corresponds to fully incoherent illumination: the field is delta-correlated in space. The limit case $\rho_o = r_o$ in which

$$\Gamma(\boldsymbol{x}, \boldsymbol{x}') = I_o \exp\Big(- \frac{|\boldsymbol{x}|^2}{r_o^2} - \frac{|\boldsymbol{x}'|^2}{r_o^2}\Big)$$

corresponds to fully coherent illumination: the spatial profile of the field is deterministic (up to a random multiplicative factor) and has a Gaussian form with radius r_o. The following proposition shows that the ghost imaging function gives an image of the square transmission function $\mathcal{T}^2$ up to an integral operator whose kernel can be identified [20].

Proposition 7.1. *If $T \to \infty$, then the ghost imaging function converges in probability to*

$$\mathcal{C}(\boldsymbol{x}) = \int_{\mathbb{R}^2} H(\boldsymbol{x}, \boldsymbol{y}) \mathcal{T}(\boldsymbol{y})^2 \mathrm{d}\boldsymbol{y}, \tag{47}$$

with the kernel given by

$$\begin{aligned} H(\boldsymbol{x}, \boldsymbol{y}) = \frac{I_o^2 \rho_o^4 r_o^4}{2^8 \pi^2 L^4} \int_{\mathbb{R}^2} \mathrm{d}\boldsymbol{\alpha} \int_{\mathbb{R}^2} \mathrm{d}\boldsymbol{\beta} \exp\Big(- \big(|\boldsymbol{\alpha}|^2 + |\boldsymbol{\beta}|^2\big)\big(1 + \frac{\omega_o^2 r_o^2 \rho_o^2}{4 c_o^2 L^2}\big)\Big) \\ \times \exp\Big(- i \frac{\omega_o}{c_o L} \big(\rho_o(\boldsymbol{x} + \boldsymbol{y}) \cdot \boldsymbol{\alpha} + r_o(\boldsymbol{x} - \boldsymbol{y}) \cdot \boldsymbol{\beta}\big)\Big) \\ \times \exp\Big(- \frac{\omega_o^2 L}{4 c_o^2} \int_0^1 2\gamma(\boldsymbol{0}) - \gamma\big((\rho_o \boldsymbol{\alpha} + r_o \boldsymbol{\beta}) s\big) - \gamma\big((\rho_o \boldsymbol{\alpha} - r_o \boldsymbol{\beta}) s\big) \mathrm{d}s\Big). \end{aligned} \tag{48}$$

If the medium is homogeneous along the two paths $\gamma = 0$, then the kernel is

$$H(\boldsymbol{x}, \boldsymbol{y}) = \frac{I_o^2 \rho_o^2 r_o^2 c_o^4}{64 \omega_o^4 \rho_{\mathrm{gi0}}^2 R_{\mathrm{gi0}}^2} \exp\Big(- \frac{|\boldsymbol{x} - \boldsymbol{y}|^2}{2\rho_{\mathrm{gi0}}^2} - \frac{|\boldsymbol{x} + \boldsymbol{y}|^2}{2R_{\mathrm{gi0}}^2}\Big), \tag{49}$$

with

$$\rho_{\mathrm{gi0}}^2 = \frac{2c_o^2 L^2}{\omega_o^2 r_o^2} + \frac{\rho_o^2}{2}, \qquad R_{\mathrm{gi0}}^2 = \frac{2c_o^2 L^2}{\omega_o^2 \rho_o^2} + \frac{r_o^2}{2}. \tag{50}$$

Eq. (50) shows that the resolution of the ghost imaging function is improved when the source becomes less coherent (i.e., when ρ_o decreases, the radius of the convolution kernel ρ_{gi0} decreases). It also shows that imaging is possible provided the object to be imaged (i.e. the support of the transmission function) is within the disk with radius R_{gi0}. This radius increases when the source becomes less coherent (i.e., when ρ_o decreases, R_{gi0} increases).

If the medium is random along the two paths and scattering is strong, in the sense that the propagation distance is larger than the scattering mean free path $L/Z_{\mathrm{sca}} \gg 1$, then

$$H(\boldsymbol{x}, \boldsymbol{y}) = \frac{I_o^2 \rho_o^2 r_o^2 c_o^4}{64 \omega_o^4 \rho_{\mathrm{gi1}}^2 R_{\mathrm{gi1}}^2} \exp\Big(- \frac{|\boldsymbol{x} - \boldsymbol{y}|^2}{2\rho_{\mathrm{gi1}}^2} - \frac{|\boldsymbol{x} + \boldsymbol{y}|^2}{2R_{\mathrm{gi1}}^2}\Big), \tag{51}$$

with

$$\rho_{\rm gi1}^2 = \frac{2c_o^2L^2}{\omega_o^2 r_o^2} + \frac{\rho_o^2}{2} + \frac{8c_o^2L^3}{3\omega_o^2 Z_{\rm sca}\ell_c^2}, \qquad R_{\rm gi1}^2 = \frac{2c_o^2L^2}{\omega_o^2 \rho_o^2} + \frac{r_o^2}{2} + \frac{8c_o^2L^3}{3\omega_o^2 Z_{\rm sca}\ell_c^2}, \tag{52}$$

and the correlation radius of the medium ℓ_c is defined as in (18).

In the partially coherent case $\rho_o \leq r_o$, formula (52) shows that the resolution is improved when the source becomes less coherent but it is degraded by scattering. Moreover, the radius of the region that can be imaged increases when the source becomes less coherent and when scattering becomes stronger. In other words, scattering degrades the resolution of the ghost imaging function, but it enhances the region that can be imaged.

In the limit case of a fully incoherent source $\rho_o \to 0$ we have $\rho_{\rm gi1}^2 \to \rho_{\rm gi}^2 := \frac{2c_o^2L^2}{\omega_o^2 r_o^2} + \frac{8c_o^2L^3}{3\omega_o^2 Z_{\rm sca}\ell_c^2}$ and $R_{\rm gi1}^2 \to +\infty$, which shows that the integral operator is then a convolution with a Gaussian kernel with radius $\rho_{\rm gi}$.

In the limit case of a fully coherent source $\rho_o = r_o$, then $\rho_{\rm gi}^2 = R_{\rm gi}^2$ and

$$H(\boldsymbol{x},\boldsymbol{y}) = \frac{I_o^2 r_o^4 c_o^4}{64\omega_o^4 R_{\rm gi}^4} \exp\Big(- \frac{|\boldsymbol{x}|^2}{R_{\rm gi}^2} - \frac{|\boldsymbol{y}|^2}{R_{\rm gi}^2}\Big),$$

with $R_{\rm gi}^2 = \frac{2c_o^2L^2}{\omega_o^2 r_o^2} + \frac{r_o^2}{2} + \frac{8c_o^2L^3}{3\omega_o^2 Z_{\rm sca}\ell_c^2}$, which has a separable form. In this case we do not get any image of the transmission function and the imaging function has a Gaussian form with width $R_{\rm gi}$ whatever the form of the transmission function. This confirms that the incoherence (or partial coherence) of the source is the key ingredient for ghost imaging.

8 Acknowledgements

I am very grateful to L. Borcea, J.-P. Fouque, G. Papanicolaou, K. Sølna, and C. Tsogka for longstanding collaborations over the years on the subjects discussed here.

References

[1] M. Asch, W. Kohler, G. Papanicolaou, M. Postel, and B. White, *Frequency content of randomly scattered signals*, SIAM Rev. **33** (1991), 519–625.

[2] F. Bailly, J.-F. Clouet, and J.-P. Fouque, *Parabolic and white noise approximation for waves in random media*, SIAM J. Appl. Math. **56** (1996), 1445–1470.

[3] G. Bal, *On the self-averaging of wave energy in random media*, SIAM Multiscale Model. Simul. **2** (2004), 398–420.

[4] G. Bal and O. Pinaud, *Dynamics of wave scintillation in random media*, Comm. Partial Differential Equations **35** (2010), 1176–1235.

[5] C. Bardos, J. Garnier, and G. Papanicolaou, *Identification of Green's functions singularities by cross correlation of noisy signals*, Inverse Problems **24** (2008), 015011.

[6] P. Blomgren, G. Papanicolaou, and H. Zhao, *Super-resolution in time-reversal acoustics*, J. Acoust. Soc. Am. **111** (2002), 230–248.

[7] L. Borcea, G. Papanicolaou, and C. Tsogka, *Interferometric array imaging in clutter*, Inverse Problems **21** (2005), 1419–1460.

[8] L. Borcea, G. Papanicolaou, and C. Tsogka, *Adaptive interferometric imaging in clutter and optimal illumination*, Inverse Problems **22** (2006), 1405–1436.

[9] L. Borcea, J. Garnier, G. Papanicolaou, and C. Tsogka, *Enhanced statistical stability in coherent interferometric imaging*, Inverse Problems **27** (2011), 085004.

[10] N. D. Cartwright, *A non-negative Wigner-type distribution*, Physica **83A** (1976), 210–212.

[11] J. F. Claerbout, *Imaging the Earth's Interior*, Blackwell Scientific Publications, Palo Alto, 1985.

[12] D. Dawson and G. Papanicolaou, *A random wave process*, Appl. Math. Optim. **12** (1984), 97–114.

[13] A. C. Fannjiang, *Self-averaging radiative transfer for parabolic waves*, C. R. Acad. Sci. Paris, Ser. I **342** (2006), 109–114.

[14] R. L. Fante, *Electromagnetic beam propagation in turbulent media*, Proc. IEEE **63** (1975), 1669–1692.

[15] S. Feng, C. Kane, P. A. Lee, and A. D. Stone, *Correlations and fluctuations of coherent wave transmission through disordered media*, Phys. Rev. Lett. **61** (1988), 834–837.

[16] M. Fink, D. Cassereau, A. Derode, C. Prada, P. Roux, M. Tanter, J. Thomas, and F. Wu, *Time-reversed acoustics*, Rep. Prog. Phys. **63** (2000), 1933–1995.

[17] J.-P. Fouque, J. Garnier, G. Papanicolaou, and K. Sølna, *Wave Propagation and Time Reversal in Randomly Layered Media*, Springer, New York, 2007.

[18] J.-P. Fouque, G. Papanicolaou, and Y. Samuelides, *Forward and Markov approximation: the strong-intensity-fluctuations regime revisited*, Waves in Random Media **8** (1998), 303–314.

[19] I. Freund, M. Rosenbluh, and S. Feng, *Memory effects in propagation of optical waves through disordered media*, Phys. Rev. Lett. **61** (1988), 2328–2331.

[20] J. Garnier, *Ghost imaging in the random paraxial regime*, Inverse Problems and Imaging **10** (2016), 409–432.

[21] J. Garnier and G. Papanicolaou, *Passive sensor imaging using cross correlations of noisy signals in a scattering medium*, SIAM J. Imaging Sciences **2** (2009), 396–437.

[22] J. Garnier and G. Papanicolaou, *Resolution analysis for imaging with noise*, Inverse Problems **26** (2010), 074001.

[23] J. Garnier and G. Papanicolaou, *Passive Imaging with Ambient Noise*, Cambridge University Press, Cambridge, 2016.

[24] J. Garnier and K. Sølna, *Random backscattering in the parabolic scaling*, J. Stat. Phys. **131** (2008), 445–486.

[25] J. Garnier and K. Sølna, *Coupled paraxial wave equations in random media in the white-noise regime*, Ann. Appl. Probab. **19** (2009), 318–346.

[26] J. Garnier and K. Sølna, *Scaling limits for wave pulse transmission and reflection operators*, Wave Motion **46** (2009), 122–143.

[27] J. Garnier and K. Sølna, *Scintillation in the white-noise paraxial regime*, Comm. Part. Differ. Equat. **39** (2014), 626–650.

[28] J. Garnier and K. Sølna, *Fourth-moment analysis for beam propagation in the white-noise paraxial regime*, Arch. Rational Mech. Anal. **220** (2016), 37–81.

[29] J. Garnier and K. Sølna, *Focusing waves through a randomly scattering medium in the white-noise paraxial regime*, SIAM J. Appl. Math. **77** (2017), 500–519.

[30] P. Gérard, P. A. Markowich, N. J. Mauser, and F. Poupaud, *Homogenization limits and Wigner transforms*, Comm. Pure Appl. Math. **50** (1997), 323–379.

[31] C. Gomez and O. Pinaud, *Fractional white-noise limit and paraxial approximation for waves in random media*, Arch. Rational Mech. Anal. **226** (2017), 1061–1138.

[32] J. W. Goodman, *Statistical Optics*, Wiley, New York, 2000.

[33] A. Ishimaru, *Wave Propagation and Scattering in Random Media*, Academic Press, San Diego, 1978.

[34] A. Ishimaru, S. Jaruwatanadilok, and Y. Kuga, *Time reversal effects in random scattering media on superresolution, shower curtain effects, and backscattering enhancement*, Radio Sci. **42** (2007), RS6S28.

[35] J. B. Keller, *Stochastic equations and wave propagation in random media*, Proc. Symp. Appl. Math. Am. Math. Soc., McGraw Hill, New York, 1964.

[36] T. Komorowski, S. Peszat, and L. Ryzhik, *Limit of fluctuations of solutions of Wigner equation*, Commun. Math. Phys. **292** (2009), 479–510.

[37] T. Komorowski and L. Ryzhik, *Fluctuations of solutions to Wigner equation with an Ornstein-Uhlenbeck potential*, Discrete Contin. Dyn. Syst. Ser. B **17** (2012), 871–914.

[38] L. Mandel and E. Wolf, *Optical Coherence and Quantum Optics*, Cambridge University Press, Cambridge, 1995.

[39] G. Manfredi and M. R. Feix, *Entropy and Wigner functions*, Phys. Rev. E **62** (2000), 4665–4674.

[40] A. P. Mosk, A. Lagendijk, G. Lerosey, and M. Fink, *Controlling waves in space and time for imaging and focusing in complex media*, Nature Photon. **6** (2012), 283–292.

[41] J. A. Newman and K. J. Webb, *Fourier magnitude of the field incident on a random scattering medium from spatial speckle intensity correlations*, Opt. Lett. **37** (2012), 1136–1138.

[42] G. Papanicolaou, *Mathematical problems in geophysical wave propagation*, Proceedings of the International Congress of Mathematicians, in 'Documanta Mathematica', Extra Volume ICM 98 I, pp. 241–265, Berlin 1998.

[43] G. Papanicolaou, L. Ryzhik, and K. Sølna, *Statistical stability in time reversal*, SIAM J. Appl. Math. **64** (2004), 1133–1155.

[44] G. Papanicolaou, L. Ryzhik, and K. Sølna, *Self-averaging from lateral diversity in the Itô-Schrödinger equation*, SIAM Multiscale Model. Simul. **6** (2007), 468–492.

[45] S. Popoff, G. Lerosey, M. Fink, A. C. Boccara, and S. Gigan, *Image transmission through an opaque material*, Nature Commun. **1** (2010), 1–5.

[46] L. Ryzhik, J. Keller, and G. Papanicolaou, *Transport equations for elastic and other waves in random media*, Wave Motion **24** (1996), 327–370.

[47] H. Sato and M. Fehler, *Wave Propagation and Scattering in the Heterogeneous Earth*, Springer-Verlag, New York, 1998.

[48] G. T. Schuster, *Seismic Interferometry*, Cambridge University Press, Cambridge, 2009.

[49] N. M. Shapiro, M. Campillo, L. Stehly, and M. H. Ritzwoller, *High-resolution surface wave tomography from ambient noise*, Science **307** (2005), 1615–1618.

[50] J. H. Shapiro and R. W. Boyd, *The physics of ghost imaging*, Quantum Inf. Process. **11** (2012), 949–993.

[51] J. W. Strohbehn, ed., *Laser Beam Propagation in the Atmosphere*, Springer, Berlin, 1978.

[52] F. Tappert, *The parabolic approximation method*, in *Wave Propagation and Underwater Acoustics*, J. B. Keller and J. S. Papadakis, eds., 224–287, Springer, Berlin (1977).

[53] V. I. Tatarski, *Wave Propagation in a Turbulent Medium*, Dover, New York, 1961.

[54] V. I. Tatarski, *The Effect of Turbulent Atmosphere on Wave Propagation*, U.S. Department of Commerce, TT-68-50464, Springfield, 1971.

[55] B. J. Uscinski, *The Elements of Wave Propagation in Random Media*, McGraw Hill, New York, 1977.

[56] B. J. Ucsinski, *Analytical solution of the fourth-moment equation and interpretation as a set of phase screens*, J. Opt. Soc. Am. A **2** (1985), 2077–2091.

[57] A. Valencia, G. Scarcelli, M. D'Angelo, and Y. Shih, *Two-photon imaging with thermal light*, Phys. Rev. Lett. **94** (2005), 063601.

[58] G. C. Valley and D. L. Knepp, *Application of joint Gaussian statistics to interplanetary scintillation*, J. Geophys. Res. **81** (1976), 4723–4730.

[59] I. M. Vellekoop and A. P. Mosk, *Focusing coherent light through opaque strongly scattering media*, Opt. Lett. **32** (2007), 2309–2311.

[60] K. Wapenaar, E. Slob, R. Snieder, and A. Curtis, *Tutorial on seismic interferometry: Part 2 - Underlying theory and new advances*, Geophysics **75** (2010), A211–A227.

[61] I. G. Yakushkin, *Moments of field propagating in randomly inhomogeneous medium in the limit of saturated fluctuations*, Radiophys. Quantum Electron. **21** (1978), 835–840.